VIROLOGY

Flavivirus induces and antagonizes antiviral RNA interference in both mammals and mosquitoes

Yang Qiu[1,2]*, Yan-Peng Xu[3]*, Miao Wang[1,2], Meng Miao[1,4], Hui Zhou[1,4], Jiuyue Xu[1,2], Jing Kong[1,2], Da Zheng[5], Rui-Ting Li[3], Rong-Rong Zhang[3], Yan Guo[3], Xiao-Feng Li[3], Jie Cui[1,2,6], Cheng-Feng Qin[3†], Xi Zhou[1,2,4†]

Mosquito-borne flaviviruses infect both mammals and mosquitoes. RNA interference (RNAi) has been demonstrated as an anti-flavivirus mechanism in mosquitoes; however, whether and how flaviviruses induce and antagonize RNAi-mediated antiviral immunity in mammals remains unknown. We show that the nonstructural protein NS2A of dengue virus-2 (DENV2) act as a viral suppressor of RNAi (VSR). When NS2A-mediated RNAi suppression was disabled, the resulting mutant DENV2 induced Dicer-dependent production of abundant DENV2-derived siRNAs in differentiated mammalian cells. VSR-disabled DENV2 showed severe replication defects in mosquito and mammalian cells and in mice that were rescued by RNAi deficiency. Moreover, NS2As of multiple flaviviruses act as VSRs in vitro and during viral infection in both organisms. Overall, our findings demonstrate that antiviral RNAi can be induced by flavivirus, while flavivirus uses NS2A as a bona fide VSR to evade RNAi in mammals and mosquitoes, highlighting the importance of RNAi in flaviviral vector-host life cycles.

INTRODUCTION

Mosquito-borne flaviviruses (genus *Flavivirus*, family Flaviviridae) are a large group of positive-stranded RNA viruses, including numerous important human pathogens such as dengue virus (DENV), Japanese encephalitis virus (JEV), Zika virus (ZIKV), West Nile virus (WNV), yellow fever virus (YFV), etc. (*1*). These viruses are transmitted between humans and mosquitoes and cause various emerging and re-emerging infectious diseases worldwide (*2*). Among them, DENV causes about 390 million human infections and 20,000 deaths annually, and the World Health Organization has listed it as one of the "Ten Threats to Global Health in 2019" (*3*). In addition, other flaviviruses have caused numerous epidemics across the globe, as the recent ZIKV outbreaks in Americas and the spread of JEV and WNV into new geographic territories have become serious threats to human health (*4*, *5*). It is estimated that over 40% of the world are at the risk of mosquito-borne flavivirus infection, and up to now, no specific antiviral therapy is available for flaviviruses (*3*, *6*).

RNA interference (RNAi) is an evolutionarily conserved post-transcriptional gene-silencing mechanism in all eukaryotes, in which small noncoding RNAs, such as small interfering RNAs (siRNAs) or microRNAs (miRNAs), direct the silencing of gene expression by causing the destruction or translational repression of complementary target RNAs, respectively (*7*). RNAi is believed to have originally evolved as an intrinsic antiviral immune mechanism in diverse eukaryotes (*7*, *8*). In the process of antiviral RNAi, viral double-stranded RNA (dsRNA) replicative intermediates (vRI-dsRNAs) produced during viral replication or dsRNAs from viral RNA secondary structures are recognized and cleaved by host endoribonuclease Dicer into 21- to 23-nucleotide (nt) virus-derived siRNAs (vsiRNAs), which are then loaded into Argonaute (AGO) proteins of the RNA-induced silencing complex (RISC), to direct the destruction of viral RNAs in infected cells (*8*, *9*). Thus far, RNAi has been widely recognized as one of the most important antiviral mechanisms in fungi, plants, and invertebrates, whereas many viruses encode viral suppressors of RNAi (VSRs) as the immune evasion strategies (*10*).

In contrast, in the differentiated mammalian cells in which viral infection and replication usually occur, vRI-dsRNAs and other viral nucleic acids mainly induce innate antiviral immune defenses, such as the interferon (IFN) system, and whether RNAi exerts any physiologically important antiviral effect in mammals has remained a long-lasting subject of debates (*11*–*13*). Recently, several lines of evidence have demonstrated that RNAi plays important antiviral roles in murine embryonic stem cells and human neural progenitor cells (hNPCs) (*14*, *15*). However, stem or progenitor cells are not the usual infection targets for most viruses, including flaviviruses. Also, in differentiated mammalian cells, a mere handful of VSR-disabled mutant viruses, including human enterovirus A71 (EV-A71), influenza A virus (IAV), and Nodamura virus (NoV), have been found to induce vsiRNA production and antiviral RNAi response during infection (*13*, *16*–*18*).

For flaviviruses, previous studies have revealed, as expected, that DENV and ZIKV can induce the production of vsiRNAs in infected *Aedes* mosquito cells (*19*–*22*). However, it still remains unknown whether RNAi exerts any antiviral effect against flavivirus infection in differentiated mammalian cells. Given the fact that mosquito-borne flaviviruses are transmitted between humans and mosquitoes, and that they carry out their life cycles in both of these organisms, determining whether and how flaviviruses induce and antagonize the shared antiviral defense mechanism, RNAi, in the two distinct host species would deepen understanding of the flavivirus processes of the infection, transmission, and pathogenesis, as well as the mechanisms of antiviral RNAi in both mammals and insects.

Flavivirus encodes a polyprotein that is further processed into three structural and seven nonstructural proteins. Here, we initially examined all the DENV2 nonstructural proteins and found that the

[1]State Key Laboratory of Virology, Wuhan Institute of Virology, Center for Biosafety Mega-Science, Chinese Academy of Sciences (CAS), Wuhan 430071, China. [2]University of Chinese Academy of Sciences, Beijing 100049, China. [3]State Key Laboratory of Pathogen and Biosecurity, Beijing Institute of Microbiology and Epidemiology, Academy of Military Medical Sciences (AMMS), Beijing 100071, China. [4]College of Life Sciences, Wuhan University, Wuhan 430072, China. [5]Beijing Institute of Technology, Beijing 10081, China. [6]CAS Key Laboratory of Molecular Virology and Immunology, Institut Pasteur of Shanghai, CAS, Shanghai 200031, China.
*These authors contributed equally to this work.
†Corresponding author. Email: qincf@bmi.ac.cn (C.-F.Q.); zhouxi@wh.iov.cn (X.Z.)

nonstructural protein NS2A suppressed Dicer-dependent siRNA production both in vitro and in the context of DENV2 infection. When the VSR activity of NS2A was disabled by reverse genetics, the resulting VSR-deficient mutant DENV2 induced abundant vsiRNA production and antiviral RNAi response in infected mammalian somatic cells. These vsiRNAs are Dicer-dependently produced from vRI-dsRNAs, loaded into AGO, and active to silence complementary viral RNA. Correspondingly, the VSR-deficient DENV2 suffered severe defects in replication and infection in mammalian somatic cells and mice, which were successfully rescued by the genetic ablation of key RNAi component. In infected *Aedes* mosquito cells, DENV2 uses the same VSR (NS2A) to antagonize antiviral RNAi, and the replication defect caused by the VSR deficiency could be also rescued by the deficiency of RNAi. In addition, NS2As of other DENV serotypes and mosquito-borne flaviviruses, including JEV, WNV, and ZIKV, also suppressed RNAi in vitro, and JEV has been found to use NS2A to antagonize antiviral RNAi in both mosquito and human cells during JEV infection. Overall, our findings demonstrate that RNAi can be triggered to exert a critical antiviral effect against flavivirus infection in both mammals and mosquitoes, while flavivirus uses NS2A as a bona fide VSR to evade antiviral RNAi in both organisms.

RESULTS

DENV2 nonstructural protein NS2A suppresses RNAi in vitro

Previous studies by us and others have implied that antiviral RNAi response and vsiRNA production would become obvious in differentiated mammalian cells infected with viruses whose VSRs are disabled by reverse genetics (*16*–*18*). Therefore, to examine whether flavivirus has the ability to induce antiviral RNAi in differentiated mammalian somatic cells, we first sought to determine whether any flaviviral protein can work as a potential VSR. To this end, we examined all DENV2 nonstructural proteins via a classic reversal-of-silencing assay. In this assay, enhanced green fluorescent protein (EGFP)–specific dsRNA was transfected into EGFP-expressing *Drosophila* S2 cells, together with expression vectors for individual DENV2 nonstructural proteins, and the levels of EGFP mRNA and protein were determined via Northern blotting and fluorescence microscopy. As shown in Fig. 1A and fig. S1 (A to C), the ectopic expression of DENV2 NS2A effectively restored the expression of EGFP mRNA and protein, indicating that NS2A is a potential VSR in insect cells. Of note, the ectopic expression of Flock House virus (FHV) B2 protein (named FB2), a well-established VSR, and the knockdown of *Drosophila melanogaster* Dicer-2 (dmDcr2-KD) or AGO2 (dmAGO2-KD) were used as positive controls, which, as predicted, inhibited the dsRNA-induced RNAi (Fig. 1A, lane 3; fig. S1A; fig. S1C, lanes 4, 6, and 7; and fig. S1D).

To further confirm the RNAi suppression activity of DENV2 NS2A, we adopted another canonical assay in S2 cells. In this assay, a VSR-deficient FHV replicon mutant (pFR1-ΔB2) was expressed to self-replicate in S2 cells (*23*). Owing to the lack of B2, this mutant FHV replicon was unable to evade antiviral RNAi, resulting in the near clearance of self-replicated FHV genomic RNA1 and subgenomic RNA3 in S2 cells, while the presence of NS2A successfully rescued the replication of FHV replicon (Fig. 1B). Together, these results showed that DENV2 NS2A is a potential VSR whose overexpression effectively suppressed RNAi in insect cells.

A key step of RNAi is the biogenesis of siRNAs from the cleavage of exogenous or endogenous dsRNAs by mammalian Dicer or insect Dicer-2 (*7*, *11*). Thus, we examined whether NS2A would affect the siRNA production from dsRNA via small RNA Northern blotting. Our data show that DENV2 NS2A inhibited the production of siRNAs from transfected dsRNAs in S2 cells (fig. S1E, lane 4). Moreover, we further examined whether NS2A binds to long dsRNA. To this end, gel shift assays were performed by incubating 0.05 μM synthetic 200-nt digoxigenin (DIG)–labeled dsRNA with increasing concentrations of recombinant maltose-binding protein (MBP)–fusion NS2A (fig. S2A). Our data show that NS2A has the in vitro dsRNA-binding activity (fig. S2B, lanes 3 to 5).

To further determine the direct role of DENV2 NS2A to protect dsRNA from Dicer-mediated cleavage, we used a classic in vitro Dicer cleavage assay, in which purified synthetic dsRNA was incubated with recombinant human Dicer (hDicer) and MBP-fusion NS2A. As shown in Fig. 1C, while dsRNA was efficiently processed into siRNAs by hDicer (lanes 2 and 3), the presence of MBP-NS2A effectively protected dsRNA from Dicer cleavage dose dependently (lanes 5 to 8). Together, we conclude that DENV NS2A suppresses RNAi by sequestrating dsRNA from Dicer cleavage in vitro.

Lysine-135 is the critical residue for the VSR activity of DENV2 NS2A

To identify the critical residue(s) responsible for the dsRNA-binding and/or RNAi suppression activities of DENV2 NS2A, we performed multiple sequence alignments of the positively charged residues of NS2As encoded by the four DENV serotypes, ZIKV, JEV, and WNV (fig. S2C) and then examined the single-point mutations of conserved arginine (R) or lysine (K) to alanine (A) via reversal-of-silencing assay. The mutational analysis revealed that the conserved R94 and K135 are critical for the in vitro VSR activity of NS2A (Fig. 1D). Furthermore, we found that either the R94A or K135A mutation almost abolished the dsRNA-binding activity of NS2A (fig. S2B, lanes 6 to 11) and failed to inhibit hDicer-mediated in vitro production of siRNA from synthetic dsRNA (fig. S2D, lanes 2 and 3), indicating that the R94 and K135 residues are critical for the in vitro VSR activity of NS2A.

We sought to generate VSR-deficient mutant viruses by introducing the R94A or K135A mutation in the NS2A coding region of the infectious clone of the DENV2 strain TSV01 (fig. S2E). The wild-type (WT; $DENV2_{WT}$) and mutant ($DENV2_{R94A}$ and $DENV2_{K135A}$) viruses were successfully recovered, and the plaque morphology was examined in baby hamster kidney-21 (BHK-21) cells (Fig. 1E). We next determined the one-step growth curve of WT and mutant DENVs in *Aedes* mosquito Aag2 and C6/36 cells. As expected, both $DENV2_{R94A}$ and $DENV2_{K135A}$ showed weaker growth patterns than did $DENV2_{WT}$ in Aag2 cells (Fig. 1F). While the replication of $DENV2_{R94A}$ and $DENV2_{K135A}$ had no significant difference in Aag2 cells (Fig. 1F), we found that the replication of $DENV2_{R94A}$ was markedly weaker than that of $DENV2_{K135A}$ in C6/36 cells (Fig. 1G). Notably, in contrast to Aag2 cells that have an intact RNAi, C6/36 cells have a dysfunctional RNAi pathway (*22*). Thus, it is suggested that the replication defect of $DENV2_{R94A}$ cannot be rescued by the RNAi incompetency in C6/36 cells, and that the R94 residue of NS2A may be involved in viral RNA replication. Given that $DENV2_{R94A}$ appears to be irresponsive to the status of RNAi in infected cells, we did not include this mutant in the subsequent studies.

VSR-deficient DENV2 induces vsiRNA production in human somatic cells

The vsiRNA production is recognized as the prerequisite of antiviral RNAi (*11*, *12*). Thus, we sought to examine the production of

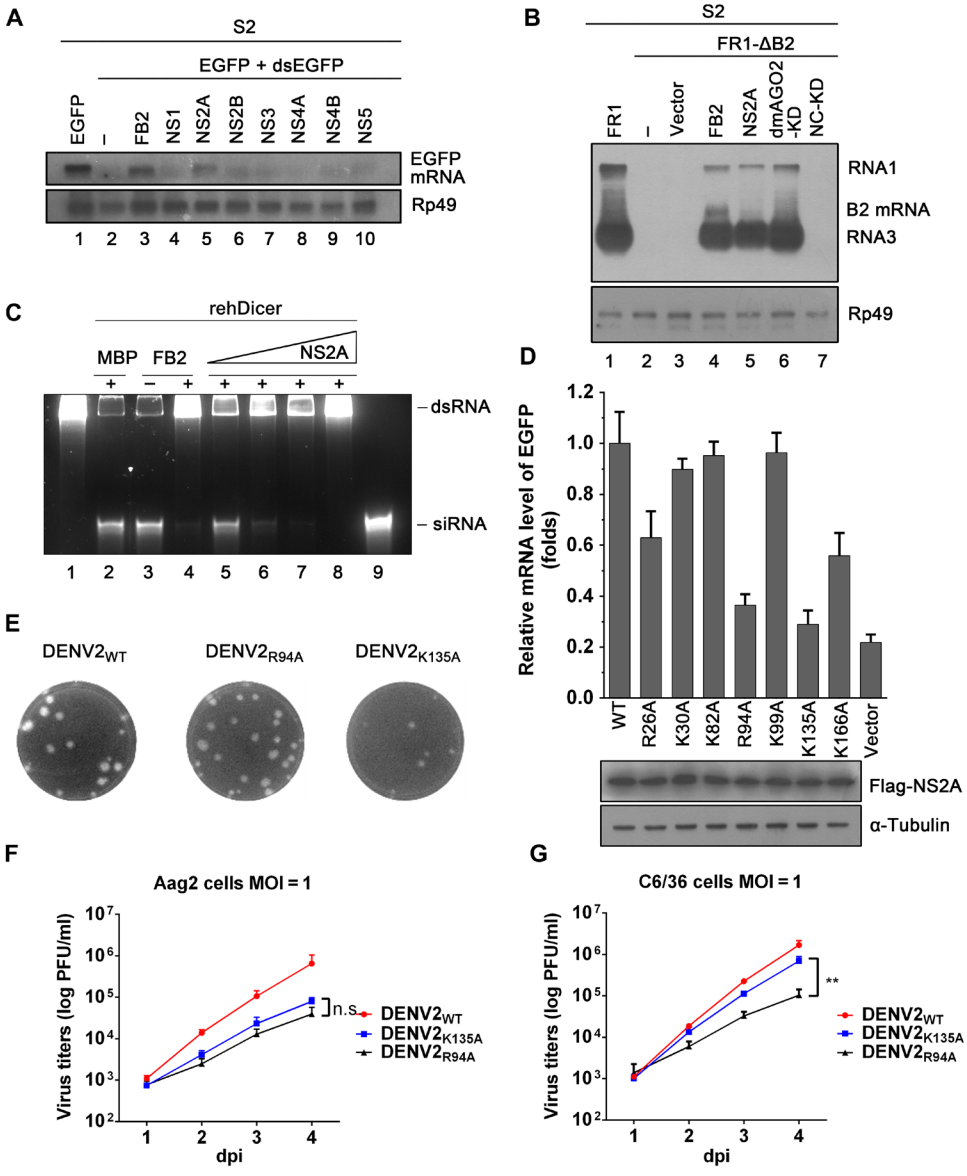

Fig. 1. DENV NS2A suppresses Dicer-mediated siRNA biogenesis. (**A**) S2 cells were cotransfected with plasmid encoding EGFP (0.3 μg), together with either an empty vector or an expression vector for FHV B2 (FB2) or DENV2 nonstructural protein (1 μg for each) as indicated. At 24 hours post-transfection (hpt), EGFP-specific dsRNA (0.1 μg) was transfected. Total RNAs were extracted at 24 hpt and subjected to Northern blotting with a digoxigenin (DIG)–labeled RNA probe targeting the 500 to 720 nt of EGFP open reading frame (ORF). Rp49 mRNA was used as a control. (**B**) S2 cells were transfected with 0.1 μg of FHV replicon (pFR1) alone or cotransfected with B2-deficient FHV replicon (pFR1-ΔB2) (1 μg) and FB2 or DENV2 NS2A (1 μg for each) as indicated. At 48 hpt, FHV RNA transcription was induced by incubation with $CuSO_4$ at 0.5 mM, and 24 hours after induction, total RNAs were extracted and subjected to Northern blotting by DIG-labeled RNA probe specific for FHV RNA1 and RNA3. The band between RNA1 and RNA3 represents the mRNA transcribed from the B2 expression vector. The dmAGO2-KD and nonspecific (NC)–knockdown (KD) cells were used as a control. (**C**) The purified FB2 or DENV2 NS2A recombinant protein was incubated with 0.4 μg of 200-nt dsRNA, together with a recombinant human Dicer (rehDicer) (0.5 U) at 37°C for 12 hours. The RNAs were separated on 7 M urea–15% polyacrylamide gel electrophoresis (PAGE) and visualized by staining with ethidium bromide. (**D**) The EGFP mRNA levels in S2 cells expressing EGFP and EGFP dsRNA, together with wild-type (WT) or indicated mutant NS2A (1 μg for each) were determined via quantitative reverse transcription polymerase chain reaction (qRT-PCR) with that in the presence of WT NS2A defined as 1. Data represent means and SD of three independent experiments. Cell lysates were subjected to Western blotting, with indicated antibodies. (**E**) The plaque morphology of $DENV2_{WT}$, $DENV2_{R94A}$, and $DENV2_{K135A}$ in BHK-21 cells. (**F** and **G**) Mosquito Aag2 or C6/36 cells were infected with $DENV2_{WT}$, $DENV2_{R94A}$, or $DENV2_{K135A}$ [multiplicity of infection (MOI) = 1]. Viral titers were measured at 1 to 4 days post-infection (dpi) using standard plaque assays in BHK-21 cells. Data represent means and SD of three independent experiments. n.s., not significant; $^{**}P < 0.01$ as measured by two-way analysis of variance (ANOVA) (GraphPad Prism).

DENV2 vsiRNAs in mammalian somatic cells infected with WT or VSR-deficient DENV2. Total RNAs were prepared from cultured human embryonic kidney (HEK) 293T cells infected with $DENV2_{WT}$ or $DENV2_{K135A}$ at a multiplicity of infection (MOI) of 10 at 3 days post-infection (dpi) and then subjected to deep sequencing. As shown in Fig. 2A, viral small RNA (vsRNA) reads from $DENV2_{WT}$-infected 293T cells did not cluster as the 22 ± 1–nt Dicer cleavage products (i.e., siRNAs) but instead were presented as predominantly nonspecific

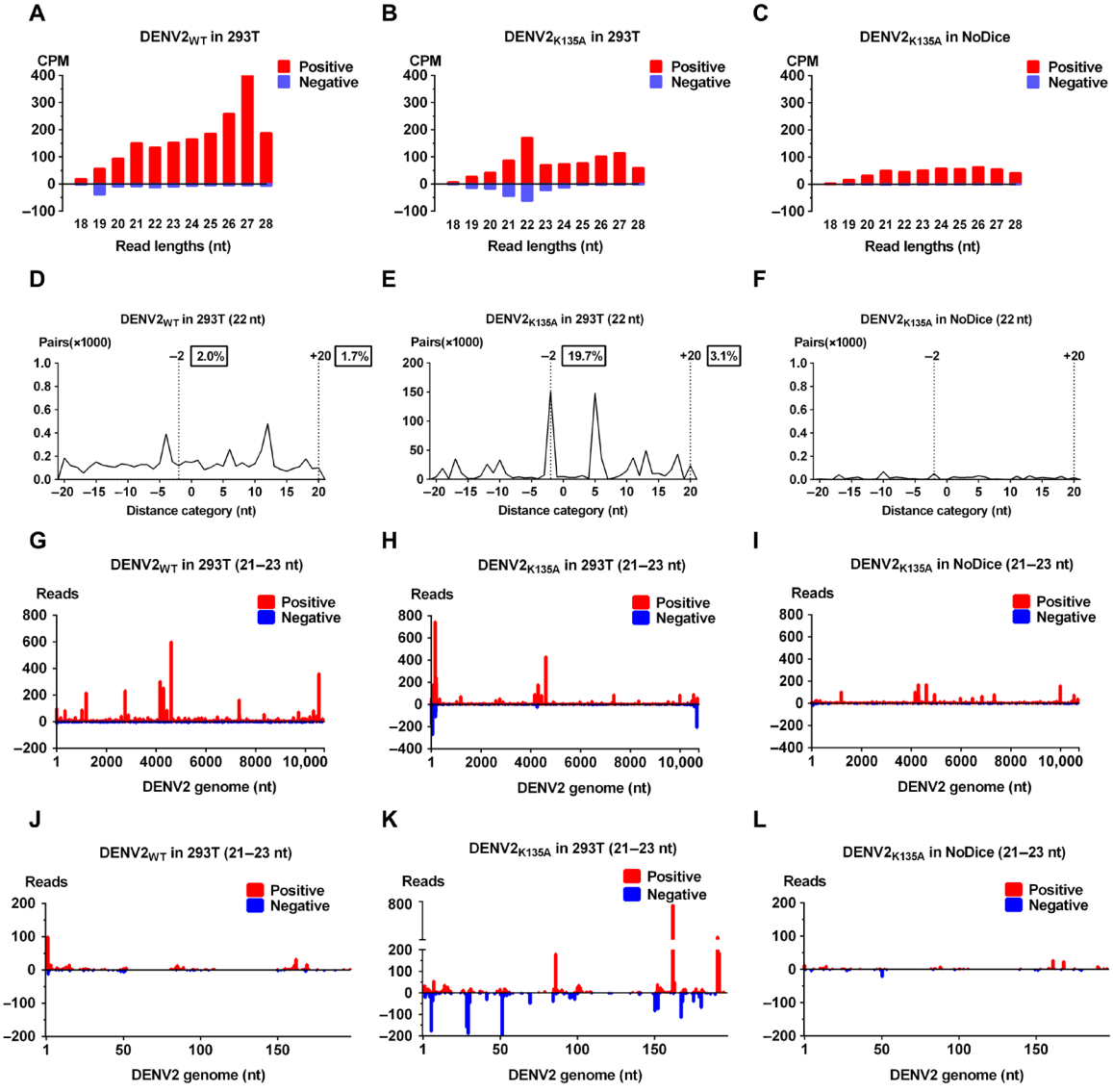

Fig. 2. Production of DENV2-derived siRNAs in human 293T cells. 293T cells were infected with $DENV2_{WT}$ (**A**, **D**, **G**, and **J**) or $DENV2_{K135A}$ (**B**, **E**, **H**, and **K**), and 293T-NoDice cells were infected with $DENV2_{K135A}$ (**C**, **F**, **I**, and **L**). RNA extracts were prepared at 3 dpi (MOI = 10) and subjected to deep sequencing. (**A** to **C**) Size distribution and abundance [counts per million of total reads (CPM)] of total vsRNAs of indicated samples. Red, (+)-vsRNAs; blue, (−)-vsRNAs. (**D** to **F**) Total pairs of complementary 22-nt vsRNAs in each distance category between 5′- and 3′-ends of a complementary vsRNA pair, shown as −2 for pairs with 2-nt overhang at the 3′-end of each strand defined as the canonical vsiRNAs; +20 indicates the distance between 5′- and 3′-ends of two consecutive vsiRNAs. The percentage of the 22-nt DENV2 vsRNA pairs with 2-nt 3′overhangs (i.e., vsiRNAs) or with 20-nt distance of two vsRNA pairs in the total 22-nt vsRNAs was indicated. (**G** to **I**) The distribution and abundance of 22 ± 1–nt (+)- and (−)-vsRNA reads mapped to the (+)- and (−)-stranded DENV2 genomes are indicated. (**J** to **L**) A close-up view of the distribution of 22 ± 1–nt vsRNA reads mapped to the 5′-terminal 200-nt region of DENV2 genome.

viral RNA degradation products with random size distribution and an overwhelming positive-strand bias, showing that no or very few vsiRNAs could be produced in $DENV2_{WT}$-infected 293T cells, consistent with previous observations (*18*, *24*).

On the other hand, when the VSR activity of NS2A was disabled by reverse genetics, the positive-strand bias of $DENV2_{K135A}$-specific vsRNA reads was substantially reduced and the proportion of negative-stranded vsRNAs in 22 ± 1–nt size was significantly improved, which shows the apparent peak of vsRNAs in 22 ± 1–nt size of both polarities in infected 293T cells (Fig. 2B and table S1). Of note, $DENV2_{K135A}$-specific vsRNA reads became less abundant than those of $DENV2_{WT}$, likely because of the greatly attenuated replication of the mutant virus. The $DENV2_{K135A}$-vsRNAs were enriched for a population of 22-nt vsRNAs that contain a 20-nt perfectly base-paired duplex with 2-nt 3′ overhangs (Fig. 2E, peak "−2"), which were not observed in the $DENV2_{WT}$-vsRNAs (Fig. 2D), showing that a significant proportion of vsRNAs with the canonical siRNA properties were produced in $DENV2_{K135A}$-infected 293T cells. $DENV2_{K135A}$-infected hDicer-deficient (NoDice) 293T cells failed to produce vsiRNAs (Fig. 2, C and F), demonstrating that the vsiRNAs production in 293T cells is Dicer dependent.

Further bioinformatic analyses revealed that $DENV_{WT}$-vsRNA reads (22 ± 1–nt size) were mainly positive stranded and distributed along the entire DENV2 genome (Fig. 2G), whereas $DENV2_{K135A}$-vsRNA

reads (22 ± 1–nt size) were highly enriched at the terminal regions of the DENV2 genome (Fig. 2H), which formed successive or phased complementary pairs of vsiRNAs (fig. S3A). A close-up view of vsiRNA presented in 1 to 200 nt of DENV2 genome also confirmed that $DENV2_{K135A}$-derived vsiRNAs were more enriched at the 5′-terminal of the genome (Fig. 2K). We speculated that without the protection of VSR, $DENV2_{K135A}$-vsiRNAs would be produced from viral genomic terminal regions where the RNA replication is initiated, consistent with the previous observations in cells infected with other WT and VSR-deficient RNA viruses like FHV, NoV, IAV, and EV-A71 (*14*, *16*–*18*).

The type I IFN (IFN-I) system is the major antiviral mechanism in mammal, and therefore, it would be intriguing to examine whether the IFN-I system has any impact on the production of vsiRNAs by using VSR-deficient DENV2. To this end, we infected IFN-α/β receptor 1 (IFNAR1)–knockout (IFNAR1-KO) 293T cells with $DENV2_{K135A}$. Similar with that in normal 293T cells, the infection of 293T-IFNAR1-KO cells with $DENV2_{K135A}$ triggered the production of abundant vsiRNAs (fig. S3B and table S1), which were also highly enriched at viral genomic terminal regions (fig. S3, C and D, peak "−2"). These results show that RNAi exerts antiviral effect irrespectively of IFN-I in human somatic cells.

We found that the percentage of the 22-nt $DENV2_{K135A}$-vsRNA pairs with 2-nt 3′overhangs (i.e., vsiRNAs) in the total 22-nt vsRNAs was higher in IFNAR1-KO 293T cells compared to that in normal 293T cells (30.7% versus 19.7%), suggesting that the IFN-I system may influence hDicer-mediated biogenesis of vsiRNAs.

In addition, the production of DENV2 vsiRNAs in 293T cells was further confirmed via Northern blotting with RNA probe complementary to 3′-end 150 to 200 nt of the negative-stranded antigenomic RNA. Consistent with the sequencing data, DENV2 vsiRNAs (22 ± 1-nt) were readily detected in 293T or IFNAR1-KO 293T cells infected with $DENV2_{K135A}$ but not with $DENV2_{WT}$, and the ablation of hDicer mostly abolished the production of vsiRNAs in 293T-NoDice cells (Fig. 3A).

Together, our findings show that when the NS2A-mediated suppression of RNAi was genetically disabled in DENV2, viral infection effectively triggered the Dicer-dependent production of abundant vsiRNAs in human somatic cells.

DENV2 vsiRNAs load into hAGO and silence cognate viral RNA sequence in human somatic cells

After demonstrating that VSR-deficient DENV2 induces vsiRNA production in 293T cells, we aimed to determine whether these vsiRNAs can load into the RISCs and be functional. Our results showed that the vsiRNAs in $DENV2_{K135A}$-infected normal or IFNAR1-KO 293T cells were coimmunoprecipitated with hAGO proteins by using an anti–pan-AGO antibody (Fig. 3A, lanes 3 and 9), indicating that $DENV2_{K135A}$ vsiRNAs can load into hAGO in human somatic cells.

Next, we sought to determine whether these vsiRNAs are able to specifically guide the degradation of cognate DENV2 genomic RNAs. To this end, we designed a plasmid that transcribes an mRNA containing *egfp* open reading frame (ORF) followed by the sequence of 1 to 200 nt of the DENV2 genome, named "EGFP-$DV_{1–200}$" (as illustrated in Fig. 3B, upper). This region of DENV2 genome is complementary with numerous vsiRNAs produced in cells infected with $DENV2_{K135A}$ as being previously detected by deep sequencing (Fig. 2). Notably, we also constructed the plasmid EGFP-$DV_{400–600}$ using the same strategy, which contains the 400 to 600 nt of the DENV2 genome but is not complementary with previously detected DENV2 vsiRNAs, as a negative control. Our results showed that the mRNA levels of EGFP-$DV_{1–200}$ were substantially reduced by infection with $DENV2_{K135A}$ but not $DENV2_{WT}$ (Fig. 3B, lanes 5 and 6). By contrast, neither $DENV2_{K135A}$ nor $DENV_{WT}$ showed any silencing effect on the mRNA of EGFP or EGFP-$DV_{400–600}$ (Fig. 3B, lanes 2 and 3 and 8 and 9), as these plasmids do not contain any vsiRNA cognate sequence. As expected, $DENV2_{K135A}$ failed to silence EGFP-$DV_{1–200}$ mRNA in 293T-NoDice cells (Fig. 3B, lane 12). Together, our data show that DENV2 vsiRNAs can effectively load into hAGO of the RISCs and guide sequence-specific silencing of cognate DENV2 RNA dependently of hDicer in human somatic cells.

Antiviral RNAi restricts DENV2 replication in human somatic cells

After determining that vsiRNA production can be triggered by infection of VSR-deficient DENV2 and be active, we examined whether RNAi exerts antiviral effect on DENV2 replication in infected human somatic cells. To this end, normal 293T and 293T-NoDice cells were infected with $DENV2_{WT}$ or $DENV2_{K135A}$. Our results showed that the deficiency of VSR resulted in substantial attenuation of viral RNA accumulation and virion production of $DENV2_{K135A}$ at 3 dpi in 293T cells (Fig. 3, C and D). Concomitantly, abundant DENV2 vsiRNAs were produced in 293T cells infected with $DENV2_{K135A}$ but not $DENV2_{WT}$ (Fig. 3A, lanes 2 and 3).

If RNAi exerts antiviral effect, then the rescue of VSR-deficient viruses should be observed in cells with the deficiency of RNAi. As shown in Fig. 3 (C and D) and fig. S4 (A and B), the replication defect of $DENV2_{K135A}$ was rescued by the deficiency of hDicer, corresponding to the abolishment of vsiRNA production in 293T-NoDice cells (Fig. 3A). Besides, loss of hDicer cannot increase the viral RNA replication of $DENV2_{WT}$ (Fig. 3, C and D), implying that RNAi is fully suppressed during DENV infection in differentiated mammalian cells. Moreover, in the absence of IFNAR1 (IFNAR1-KO), the deficiency of hDicer could further enhance $DENV2_{K135A}$ replication (Fig. 3, C and D), further confirming that RNAi exerts antiviral effect irrespectively of IFN-I.

Together, our findings show that the VSR-deficient DENV2 can be rescued in RNAi-deficient human somatic cells, and the rescuing effect well corresponds to the inhibition of vsiRNA production and is irrespective of the IFN-I system.

Antiviral RNAi restricts DENV2 replication in mammalian primary somatic cells and mice

We aim to expand our investigations of the antiviral effects of RNAi in primary cells and mouse models. For this purpose, primary murine lung fibroblasts (MLFs) were isolated from 8-week-old WT or *Ifnar1*$^{-/-}$ C57/B6 mice and infected with $DENV2_{WT}$ or $DENV2_{K135A}$. Our results showed that the deficiency of VSR substantially attenuated the viral RNA replication and virion production in WT or *Ifnar1*$^{-/-}$ MLFs at 3 dpi (Fig. 4, A and B), in agreement with our observations in human cell lines. Moreover, infection with $DENV2_{K135A}$ but not $DENV2_{WT}$ triggered the production of vsiRNAs, which were readily detectable via Northern blotting, in WT or *Ifnar1*$^{-/-}$ MLFs (Fig. 4C, lanes 2, 3, 8, and 9). In addition, the vsiRNAs produced in $DENV2_{K135A}$-infected WT or *Ifnar1*$^{-/-}$ MLFs could also load into murine AGO (mAGO) as being revealed via the RNA–immunoprecipitation (IP) assay (Fig. 4D, lanes 3 and 6).

Consistent with our observations in human 293T cells (Fig. 3), the knockdown of murine Dicer (mDicer-KD) rescued the viral RNA accumulation and virion production of $DENV2_{K135A}$ in either WT or *Ifnar1*$^{-/-}$ MLFs (Fig. 4, A and B). These data further confirm

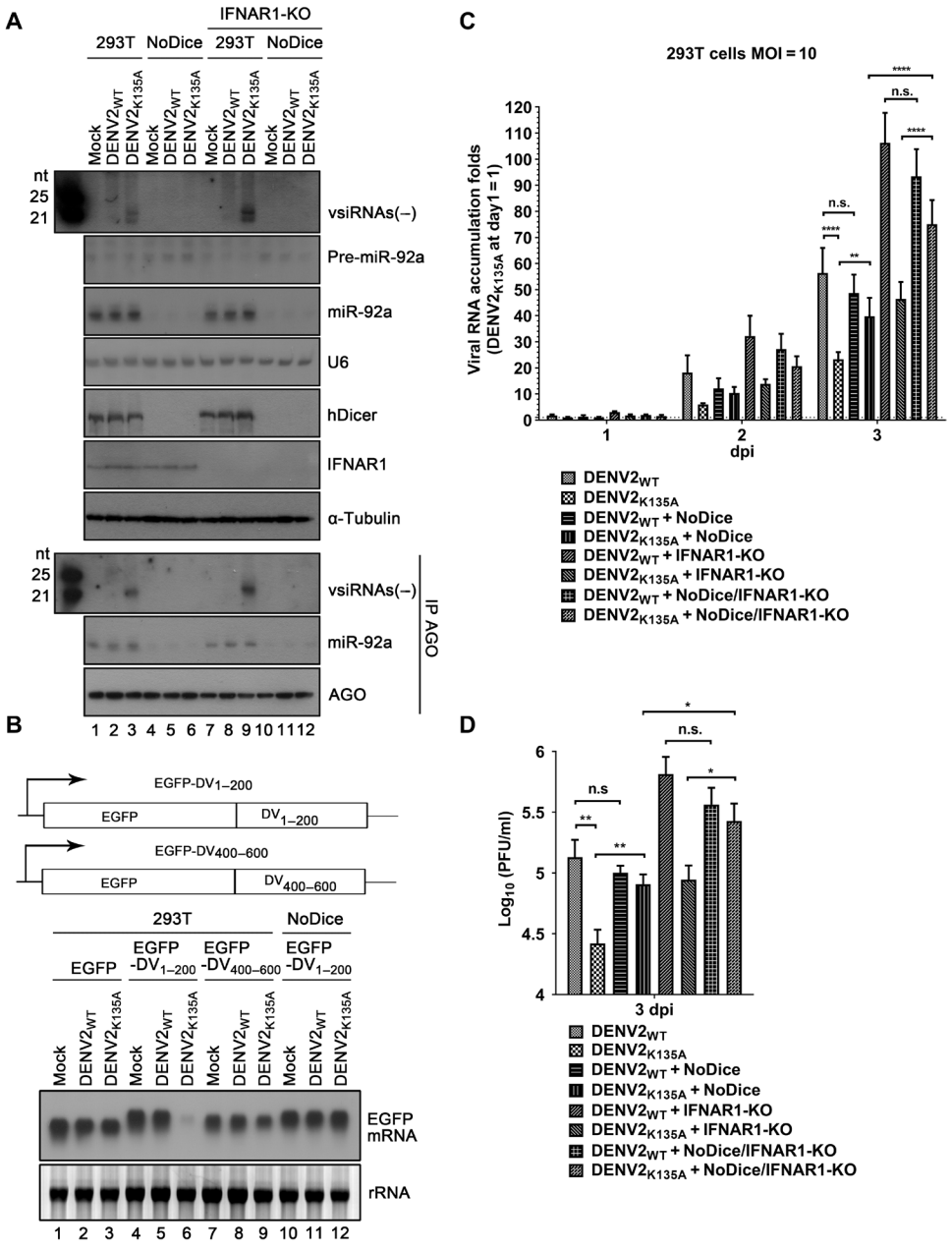

Fig. 3. NS2A works as a potent VSR during DENV infection in human 293T cells. (**A**) 293T, 293T-NoDice, 293T-IFNAR1-KO, or 293T-NoDice/IFNAR1-KO cells were infected with the same titer (MOI = 10) of $DENV2_{WT}$ or $DENV2_{K135A}$ at 3 dpi, and the vsiRNAs were detected via Northern blotting by using a DIG-labeled RNA probe complementary to 150 to 200 nt of the (–)-stranded antigenomic RNA. The same set of RNA and protein samples were used for Northern or Western blotting to detect indicated RNAs or proteins. The same cell lysates were subjected to RNA–immunoprecipitation (IP) with anti–pan-AGO antibody, and Western and Northern blotting were performed to detect precipitated hAGO and hAGO-bound vsiRNAs. The synthetic 21- and 25-nt RNAs were used as size markers. (**B**) Schematic diagram of the plasmid that transcribes the mRNA containing the *egfp* ORF followed by the 1 to 200 or 400 to 600 nt of DENV2 genome (EGFP-$DV_{1–200}$ and EGFP-$DV_{400–600}$) (top). 293T or 293T-NoDice cells were transfected with the indicated plasmid, and at 2 hpt, cells were infected with $DENV2_{WT}$ or $DENV2_{K135A}$. At 3 dpi, total RNAs were extracted and subjected to Northern blotting to detect EGFP mRNA. rRNA, ribosomal RNA. (**C** and **D**) 293T, 293T-NoDice, 293T-IFNAR1-KO, or 293T-NoDice/IFNAR1-KO cells were infected with $DENV2_{WT}$ or $DENV2_{K135A}$ as indicated. At 1 to 3 dpi, the levels of DENV2 genomic RNAs were determined via qRT-PCR, as the level of $DENV2_{K135A}$ RNA in 293T cells at 1 dpi was defined as 1 (C). The viral titers at 3 dpi were determined (**D**). All data represent means and SD of three independent experiments. The qRT-PCR and viral titer data were measured via two-way ANOVA and *t* test (GraphPad Prism), respectively. $*P < 0.05$, $**P < 0.01$, $****P < 0.0001$.

the rescuing effect of the loss of Dicer on VSR-deficient DENV2 and indicate that it is not attributed to IFN-I. In addition, the production of vsiRNAs was dependent on the presence of mDicer in both WT and *Ifnar1*$^{-/-}$ MLFs as expected (Fig. 4C, lanes 6 and 12).

Moreover, we assessed the effect of VSR deficiency on viral replication in vivo by infecting littermates of *Ifnargr*$^{-/-}$ mice (AG6) that lack IFN-I/II receptors with 1×10^4 plaque-forming units (PFU) of WT or VSR-deficient mutant of DENV2 via intracerebral injection.

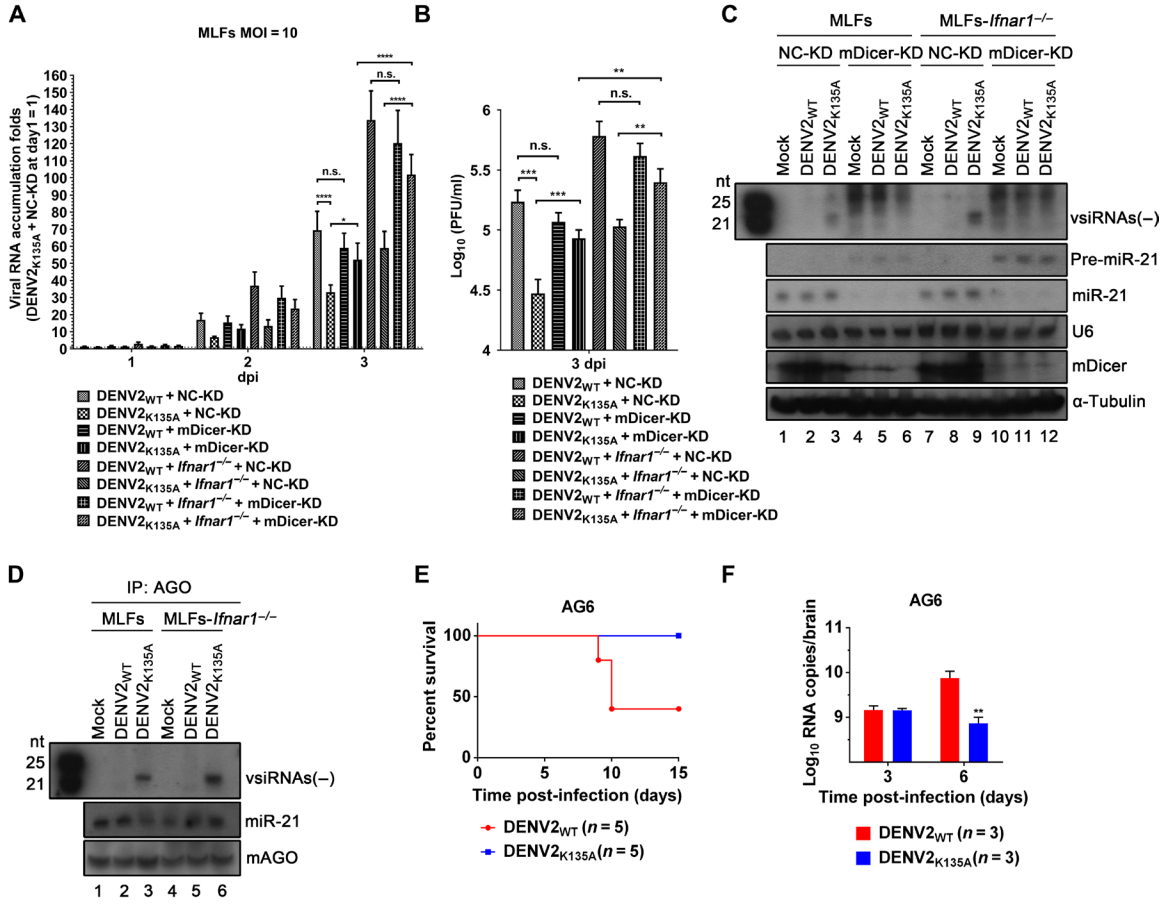

Fig. 4. The deficiency of VSR causes replication and infection defects in DENV2-infected murine primary cells and mice. (**A** and **B**) Primary WT or *Ifnar1*$^{-/-}$ MLFs with or without mDicer knockdown (mDicer-KD) were infected with $DENV2_{WT}$ or $DENV2_{K135A}$ at an MOI of 10. At 1 to 3 dpi, the levels of DENV2 RNAs were measured via qRT-PCR, as the level of $DENV2_{K135A}$ RNA in WT MLFs at 1 dpi was defined as 1 (A). The viral titers at 3 dpi were determined (B). All data represent means and SD of three independent experiments. The qRT-PCR and viral titer results were measured by two-way ANOVA and *t* test (GraphPad Prism), respectively. *$P < 0.05$, **$P < 0.01$, ***$P < 0.001$, ****$P < 0.0001$. (**C** and **D**) WT or *Ifnar1*$^{-/-}$ MLFs with or without mDicer-KD were infected with $DENV2_{WT}$ or $DENV2_{K135A}$ (MOI = 10). At 3 dpi, total RNA extracts and cell lysates were prepared and subjected to Northern and Western blotting to detect indicated RNAs and proteins (C). The same set of samples were subjected to RNA-IP with anti–pan-AGO antibody, followed by Western and Northern blotting to detect precipitated mAGO and mAGO-bound vsiRNAs, respectively (D). (**E**) Littermates of 3-week-old *Ifnargr*$^{-/-}$ AG6 mice were intracerebrally injected with 1×10^4 PFU of $DENV2_{WT}$ ($n = 5$) or $DENV2_{K135A}$ ($n = 5$). The mortalities were monitored for 15 days or until death. (**F**) Littermates of 3-week-old *Ifnargr*$^{-/-}$ AG6 mice intracerebrally injected with 1×10^4 PFU of $DENV2_{WT}$ or $DENV2_{K135A}$. Mouse brains at 3 and 6 dpi were collected and homogenized. The levels of viral RNA were measured via qRT-PCR. **$P < 0.01$ as measured by two-way ANOVA (GraphPad Prism).

The mortalities of the infected mice were monitored for 15 days. Our data show that $DENV2_{WT}$ infection resulted in 60% mortality of the infected mice within 10 days, whereas $DENV2_{K135A}$-infected mice all survived at 15 dpi (Fig. 4E). In addition, mouse brains derived from AG6 mice infected with WT or mutant virus at 3 and 6 dpi were extracted and the viral RNA accumulations were determined, showing that the replication of VSR-deficient DENV2 was substantially restricted compared to that of $DENV2_{WT}$ (Fig. 4F). Moreover, we repeated the in vivo assays in littermates of Balb/c mice using the same viruses and obtained similar results (fig. S4, A and B).

Together, in agreement with that in human somatic cells, the ex vivo and in vivo data show that VSR-deficient DENV2 triggered the production of readily detectable vsiRNAs, which well corresponds with substantial attenuation of viral replication and pathogenicity, in a Dicer-dependent but IFN-I–irrespective manner.

NS2A regulates the biogenesis of DENV2 vsiRNAs in *Aedes* mosquito cells

After determining that RNAi exerts the antiviral effect and NS2A works as a bona fide VSR in the context of DENV infection in differentiated mammalian cells, we sought to examine whether DENV2 uses the same mechanism to evade antiviral RNAi in infected mosquito cells. Our previous data showed that DENV2 NS2A does have in vitro VSR activity in insect cells (Fig. 1). Thus, we infected mosquito Aag2 cells with $DENV2_{WT}$ or $DENV2_{K135A}$ (MOI = 10). Total RNAs were extracted at 3 dpi and then subjected to deep sequencing. Since antiviral RNAi is predominant in insects, it was not surprising to find a dominant pattern of vsiRNAs, i.e., 21-nt vsRNA reads with an almost equal ratio of positive and negative strands, in $DENV2_{WT}$-infected Aag2 cells (Fig. 5A and table S1). These vsiRNA pairs were distributed along the entire DENV2 genome (Fig. 5B). These data show that like insect viruses, $DENV2_{WT}$ can induce the production of abundant vsiRNA in mosquito cells even in the presence of VSR.

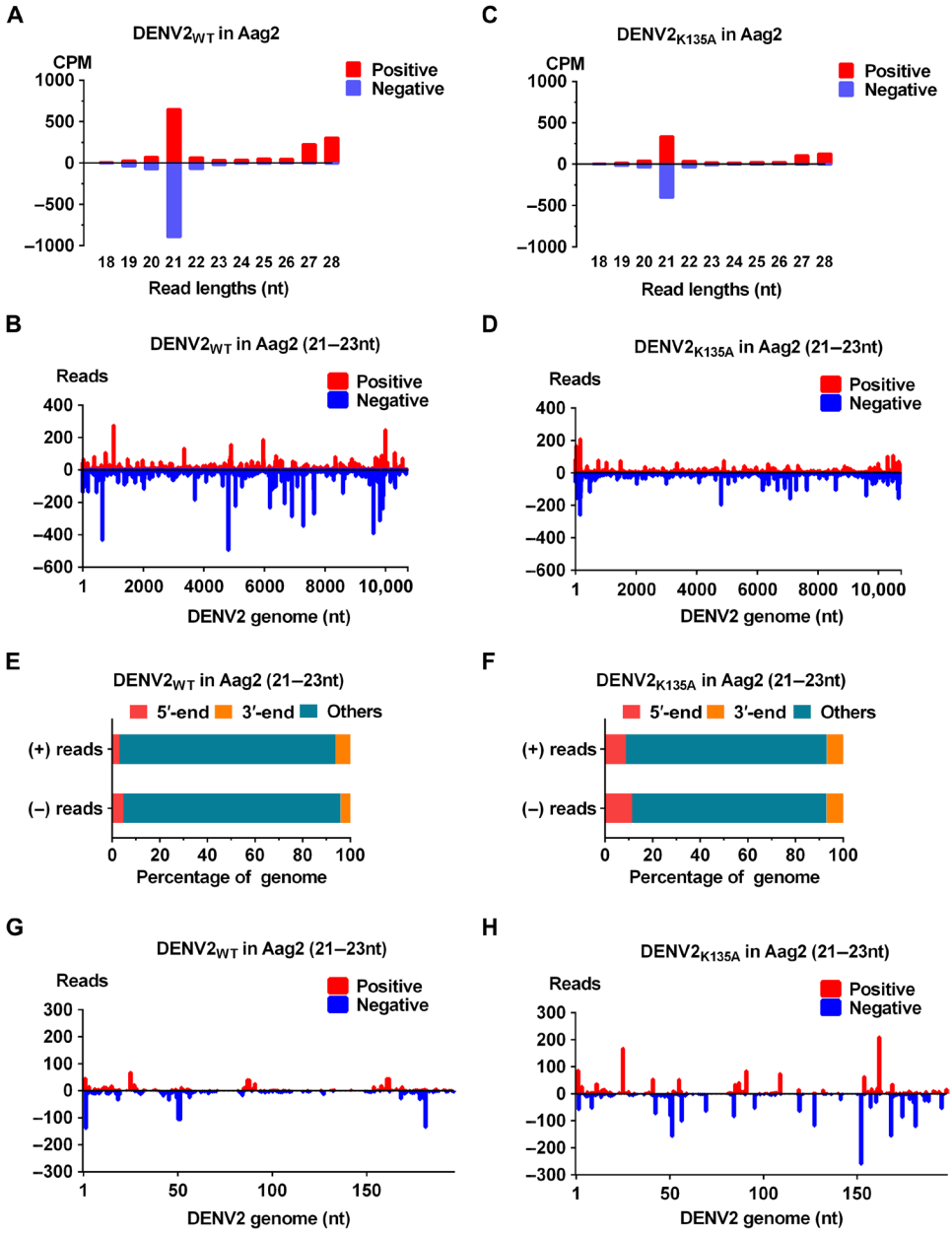

Fig. 5. Production of DENV2-derived vsiRNAs in mosquito Aag2 cells. (**A** to **D**) Size distribution and abundance (CPM) of total vsRNAs sequenced from Aag2 cells infected with $DENV2_{WT}$ (A) or $DENV2_{K135A}$ (C) at an MOI of 10 at 3 dpi. Red, (+)-vsRNAs; blue, (–)-vsRNAs. The distribution of 22 ± 1–nt vsRNA reads mapped to the (+)- and (–)-stranded $DENV2_{WT}$ (B) or $DENV2_{K135A}$ (D) genome and the relative abundances of (+)- and (–)-stranded vsRNAs are indicated. (**E** to **F**) The percentage of 22 ± 1–nt vsRNAs mapped to the 5′-terminal (1 to 200 nt) and 3′-terminal (10,226 to 10,725 nt) regions of $DENV2_{WT}$ (E) or $DENV2_{K135A}$ (F) were highlighted as red and orange, respectively. (**G** and **H**) A close-up view of the distribution of 22 ± 1–nt vsRNA reads mapped to the 5′-terminal 200-nt region of $DENV2_{WT}$ (G) or $DENV2_{K135A}$ (H) genome.

In the context of $DENV2_{K135A}$ infection, vsRNA reads were also presented as a dominant 21-nt size and divided approximately equally into positive and negative strands (Fig. 5C and table S1), while vsRNA reads in $DENV2_{K135A}$-infected cells were less abundant than those in $DENV2_{WT}$-infected cells (Fig. 5C) likely because of the reduced viral RNA replication of the mutant virus. The analysis of the genomic origin of the vsiRNAs (21-nt size) showed that $DENV2_{K135A}$-derived vsiRNAs were more concentrated at the 5′ and 3′ termini of the DENV2 genome than did $DENV2_{WT}$-derived vsiRNAs (Fig. 5, D to F), consistent with our sequencing data in the DENV2-infected mammalian cells (Fig. 2). A close-up view of vsiRNA presented in 1 to 200 nt of DENV2 genome also confirmed that $DENV2_{K135A}$-derived vsiRNAs were more enriched at the 5′ termini of the genome (Fig. 5, G and H).

Moreover, vsiRNAs from $DENV2_{WT}$- or $DENV2_{K135A}$-infected Aag2 cells were detected via Northern blotting with the probe complementary to 3′-end 150 to 200 nt of DENV2 antigenome (Fig. 6A, lanes 2 and 3). Consistent with the sequencing data, the

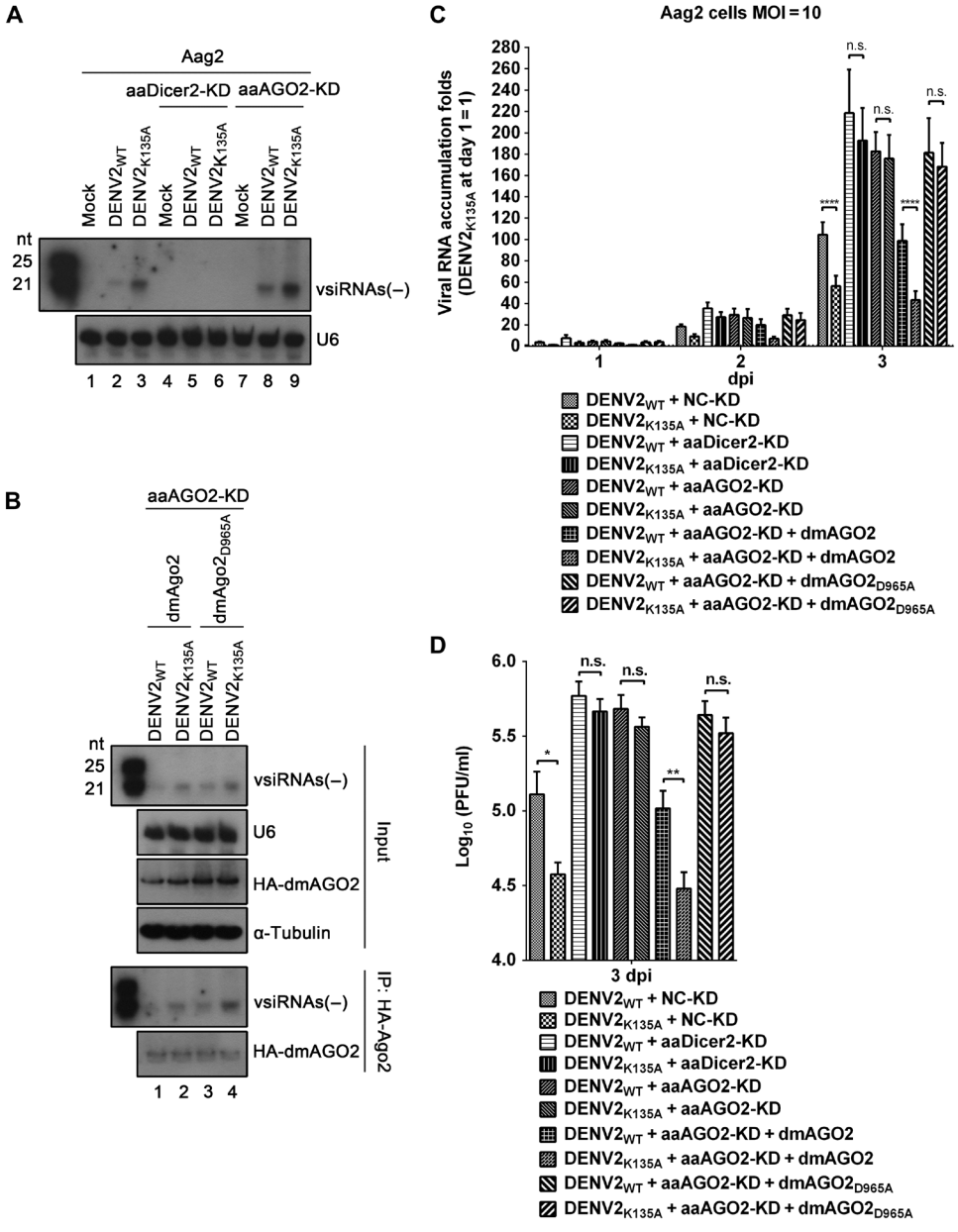

Fig. 6. NS2A works as a potent VSR during DENV infection in mosquito cells. (**A**) Northern blotting of vsiRNAs in NC-KD, aaDicer2-KD, or aaAGO2-KD Aag2 cells infected with $DENV2_{WT}$ or $DENV2_{K135A}$ at an MOI of 10 at 3 dpi. U6 was used as a loading control. (**B**) The aaAGO2-KD Aag2 cells expressing dmAGO2 or $dmAGO2_{D965A}$ were infected with $DENV2_{WT}$ or $DENV2_{K135A}$ (MOI = 10). At 3 dpi, the cell lysates were subjected to RNA-IP with anti-HA antibody. Input and precipitated small RNAs or proteins were detected by Northern or Western blotting via indicated probes or antibodies, respectively. (**C** and **D**) NC-KD, aaDicer2-KD, or aaAGO2-KD Aag2 cells in the absence or presence of ectopically expressed dmAGO2 or $dmAGO2_{D965A}$ were infected with $DENV2_{WT}$ or $DENV2_{K135A}$ (MOI = 10) as indicated. At 1 to 3 dpi, the levels of DENV2 genomic RNAs were determined via qRT-PCR. The level of $DENV2_{K135A}$ RNA in Aag2 cells at 1 dpi was defined as 1 (C). The viral titers at 3 dpi were determined (D). All data represent means and SD of three independent experiments. The qRT-PCR and viral titer results were measured by two-way ANOVA and *t* test (GraphPad Prism), respectively. $^*P < 0.05$, $^{**}P < 0.01$, $^{***}P < 0.001$, $^{****}P < 0.0001$.

detected level of $DENV2_{K135A}$-vsiRNAs was higher than that of $DENV2_{WT}$-derived siRNAs (Fig. 6A, lanes 2 and 3), because more vsiRNAs were located at the 5′ termini of $DENV2_{K135A}$ genome than that of $DENV2_{WT}$ (Fig. 5, E to H). Together, our data indicate that NS2A plays a protective role on the terminal regions of vRI-dsRNAs from Dicer-2 cleavage in DENV2-infected Aag2 cells.

NS2A works as a bona fide VSR during DENV2 infection in mosquito cells

After determining the protective role of NS2A on vRI-dsRNA terminal regions, we further examined some fundamental characteristics of these DENV2 vsiRNAs. Our data show that the production of either $DENV2_{WT}$- or $DENV2_{K135A}$-derived vsiRNAs was mostly abolished by the knockdown of *Aedes aegypti* Dicer-2 (aaDcr2-KD) but not

AGO2 (aaAGO2-KD) (Fig. 6A, lanes 4 to 9, and fig. S5, A and B). In addition, since no anti-aaAGO2 antibody is available, we replaced endogenous aaAGO2 with a hemagglutinin (HA)–tagged dmAGO2 by ectopically expressing HA-dmAGO2 in aaAGO2-KD Aag2 cells. These cells were infected with $DENV2_{WT}$ or $DENV2_{K135A}$, and the vsiRNAs derived from either virus were coimmunoprecipitated with dmAGO2 (Fig. 6B, lanes 1 and 2). In addition, previous studies have uncovered that the DDH motif, particularly its first aspartic acid (D597), of human AGO2 (hAGO2) is required for the slicing but not siRNA-loading activity of hAGO2. Given that this residue is also conserved in AGO proteins of other organisms, including fruit fly and *Aedes* mosquito (fig. S5C), we generated the dmAGO2 mutant by substituting the first aspartic acid of the DDH motif to alanine ($dmAGO2_{D965A}$). Our results show that vsiRNAs could also load into $dmAGO2_{D965A}$ in either WT or mutant DENV2–infected aaAGO2-KD Aag2 cells (Fig. 6B, lanes 3 and 4). Thus, these DENV2 vsiRNAs, either derived from WT or VSR-deficient mutant, are Dicer-2–dependently produced from vRI-dsRNAs and can effectively load into AGO2 of the RISC to be functional in mosquito cells.

Next, we examined whether the VSR activity of NS2A facilitates DENV2 replication in Aag2 cells. Our data show that the viral RNA accumulation and virion production of $DENV2_{K135A}$ were significantly attenuated at 3 dpi in Aag2 cells (Fig. 6, C and D). Impairing RNAi by knocking down aaDicer2 or aaAGO2 or by inactivating the slicing activity of AGO2 (i.e., replacing aaAGO2 with $dmAGO2_{D965A}$) successfully rescued the viral RNA accumulation and virion production of $DENV2_{K135A}$ to the similar levels of $DENV2_{WT}$ (Fig. 6, C and D), showing that the protective role of NS2A on DENV2 replication in mosquito cells is dependent on the RNAi pathway. Together, our findings demonstrate that in *Aedes* mosquito cells, DENV2 uses the same strategy, i.e., NS2A as bona fide VSR, to evade antiviral RNAi in the context of viral infection.

Multiple flaviviruses use NS2A as VSR to antagonize RNAi

Our previous sequence analysis revealed that NS2As from all the four DENV serotypes (DENV1-4) and multiple other flaviviruses share high homology in amino acid sequences (fig. S2C), suggesting their commonalities in functions. Thus, we first examined whether NS2As from DENV serotype-1 to serotype-4 have the same VSR activities. Our data show that ectopically expressing any of the four NS2As showed similar in vitro RNAi suppression activities in both S2 (fig. S6, A and B) and Aag2 cells (fig. S6, C and D). After that, we further assessed the VSR activity of NS2A encoded by ZIKV, JEV, or WNV in 293T cells, in which RNAi is induced by an EGFP-specific small hairpin RNA (shRNA), and found that NS2As encoded by these viruses had similar in vitro RNAi suppression activities to restore EGFP mRNA and inhibit siRNA production (fig. S7). Thus, our data show a conserved role of NS2A as a potential VSR for all the DENV serotypes as well as multiple other flaviviruses.

It would be intriguing to investigate whether these flaviviruses also use NS2A as a bona fide VSR to evade antiviral RNAi in the context of viral infection. On the basis of the sequence alignment of flaviviral NS2As, the K135 of DENV2 NS2A corresponds to the R140 of JEV NS2A (fig. S2C), both of which are positively charged. Thus, we introduced the R140A mutation in the NS2A coding region of the infectious clone of the JEV strain SA-E70 (fig. S8A) and recovered the WT (JEV_{WT}) and mutant (JEV_{R140A}) viruses. The plaque morphology was examined in BHK-21 cells (fig. S8B). We further infected mosquito Aag2 or C6/36 cells and human 293T or 293T-NoDice cells with JEV_{WT} or JEV_{R140A} and examined viral replication. Consistent with the data obtained using WT and VSR-deficient DENV2 (Figs. 3 and 6), JEV_{R140A} exhibited a replication defect in the RNAi-competent Aag2 or 293T cells when being compared to JEV_{WT} (fig. S8, C and E). On the other hand, impairing RNAi rescued the replication defect of JEV_{R140A} in both mosquito and mammalian somatic cells, as the replication of JEV_{WT} and JEV_{R140A} in RNAi-incompetent C6/36 or 293T-NoDice cells showed no significant difference (fig. S8, D and F). These data imply that RNAi can exert antiviral effect against JEV infection in both mammalian and mosquito cells, and JEV NS2A also works as a bona fide VSR to antagonize antiviral RNAi during JEV infection of either host cells.

DISCUSSION

Antiviral RNAi is an intrinsic immune defense mechanism conserved in diverse eukaryotic organisms. Vector-borne viruses, such as mosquito-borne flaviviruses, infect and replicate in both invertebrates and mammals. However, although flaviviruses have been previously revealed to induce vsiRNA production in insect cells (*19*–*22*), it was unknown whether these viruses also induce vsiRNA production and antiviral RNAi in differentiated mammalian cells and whether and how flaviviruses use certain strategy to evade antiviral RNAi in the context of viral infection in both mammals and mosquitoes.

Previous studies have implied that the unavailability of ample vsiRNAs in virus-infected–differentiated mammalian cells is probably due to the presence of potent VSRs (*14*, *16*–*18*), and thus, disabling VSR may be a useful way to assess whether RNAi exerts antiviral effect against certain viruses (*12*). Similar with the well-characterized VSR–EV-A71 3A, flaviviral NS2A is also a small (~22 kDa) transmembrane protein, which participates in viral RNA replication and virion assembly, and antagonizes IFN response (*25*–*31*); and ZIKV NS2A has been recently found to interact with and deplete adherens junction proteins in radial glial cells (*32*). On the other hand, the VSR activity of flaviviral NS2A was not assessed before. In the current study, we first identified DENV2 NS2A as a potential VSR via a set of in vitro assays. Then, when NS2A's VSR activity was disabled by reverse genetics, VSR-deficient DENV2 induced abundant vsiRNA production and antiviral RNAi response in infected mammalian somatic cells, resulting in attenuated viral replication and infection compared to the WT. The replication defect caused by disabling VSR can be rescued by impairing the RNAi machinery in an IFN-irrespective manner, demonstrating that RNAi does exert antiviral effect against DENV2 infection in differentiated mammalian cells. NS2A also acts as a bona fide VSR during DENV2 infection of *Aedes* mosquito cells. Using NS2A as VSR is a common strategy for multiple flaviviruses to evade antiviral RNAi.

Previous studies have found that DENV NS2A is associated with endoplasmic reticulum (ER) and contains eight predicted transmembrane segments (pTMS1 to pTMS8) (*30*). Moreover, scanning mutagenesis studies of NS2A implicated that the intermolecular interactions between pTMSs are critical in a DENV life cycle (*25*, *33*). Mutations of multiple conserved residues in different pTMSs, which are located inside or outside the ER lumen or within the ER membrane, showed different defect patterns (*25*, *33*). K135 of NS2A is predicted to locate in pTMS5 at the lumen side of ER (*30*), which possibly involves NS2A VSR function by mediating pTMS interactions.

In addition to NS2A, an interesting question is whether flaviviruses encode another VSR(s). Previous studies have identified some flaviviral factors, including WNV subgenomic flavivirus RNA (sfRNA) and DENV NS4B, that suppressed synthetic dsRNA- or shRNA-induced RNAi via in vitro assays (*34*, *35*). Besides, Myles and colleagues genetically added a YFV capsid gene into the genome of Sindbis virus (SINV) and observed that the mutant SINV overexpressing YFV capsid exhibited enhanced viral replication and virulence in mosquito, while the mutant SINV overexpressing DENV NS4B or WNV sfRNA failed to do so (*36*), suggesting that flaviviral capsid has the potential to be a VSR. However, these in vitro studies did not assess whether these flaviviral factors affect vsiRNA production or antiviral RNAi in the context of authentic flaviviral infection. Moreover, the assays relying on overexpressing a candidate VSR have an inherent caveat, as the overexpression of a protein with potent dsRNA-binding capacity may interfere with RNAi anyhow, which does not necessarily mean that it really works as a bona fide VSR during viral infection. On the other hand, it is expected that a virus can encode more than one antagonist of a given immune mechanism. For example, multiple flaviviral proteins have been found to be IFN antagonists (*26*). Thus, the potential VSR activities of these flaviviral factors is worth further investigation in the context of viral infection in the future.

Although RNAi is conserved in all eukaryotes, a long-standing question is why infection with multiple WT viruses fails to trigger abundant vsiRNA production in differentiated mammalian cells but can readily do so in insect cells. A reasonable explanation is that insect has a stronger Dicer machinery to process vRI-dsRNA. However, previous findings using different insect viruses and mammalian viruses are inappropriate to be directly compared and cannot exclude a less likely possibility that mammalian viruses encode more potent VSRs to block vsiRNA production. Therefore, mosquito-borne flaviviruses, which have dual life cycles, are ideal models to study antiviral RNAi in the two distinct organisms. Moreover, it would be intriguing to know whether a flavivirus uses the same or different strategy to evade RNAi in mammals and insects. Our findings show that flaviviruses use the same strategy (NS2A as VSR) to antagonize RNAi in both organisms, and antiviral RNAi does seem more prominent in insect cells than in mammalian somatic cells.

Why does antiviral RNAi respond to the same flavivirus less effectively in differentiated mammalian cells than in insect cells? A probable mechanism is that mammalian Dicer bears some intrinsic inhibition(s). Factually, it has been found that the N-terminal helicase domain of hDicer can autoinhibit its siRNA processing activity (*24*), while dmDicer-2 could partially reconstitute dsRNA-induced RNAi in human somatic cells (*37*);.the difference in the N termini of hDicer and dmDicer-2 may reflect their different capabilities in processing long dsRNA (*38*). In addition, cellular signalings may also repress antiviral RNAi in certain circumstances (*39*, *40*). Maillard *et al.* (*41*) have revealed that the IFN-I system inhibits dsRNA-induced RNAi in mammalian somatic cells via the association of the RIG-like receptor LGP2 with Dicer. However, inactivation of IFN-I response by depleting RIG-I and MDA5 is insufficient to enable vsiRNA production in human somatic cells infected with several WT RNA viruses (*42*), which we also observed in DENV2$_{WT}$-infected IFNAR1-KO cells. Such a discrepancy is probably attributed to the interference of VSRs. A recent study by us uncovered that infection with WT ZIKV could induce the production of abundant vsiRNAs in hNPCs, which lack IFN-I response, but not in neurons differentiated from hNPCs, implying that hDicer machinery and antiviral RNAi are highly tunable and differently regulated during distinct stages of cell differentiation (*15*, *43*). Future studies should elucidate the cellular determinants of the different states of antiviral RNAi in detail.

To our best knowledge, this study is the first to demonstrate that a flavivirus can trigger abundant vsiRNA production and effective antiviral RNAi response in a Dicer-dependent manner in differentiated mammalian cells. Moreover, it provides the mechanistic insight into how flaviviruses act to evade antiviral RNAi in the context of viral infection of both mammals and mosquitoes. These findings extend our knowledge about the life and transmission cycles of mosquito-borne flaviviruses and shed light onto the interaction between this large group of pathogenic viruses and antiviral RNAi immunity, which may be amenable to antiviral therapy and would represent an exciting avenue for future studies.

MATERIALS AND METHODS

Cell culture

The *Drosophila* S2 cells and *A. aegypti* cell line Aag2 [American Type Culture Collection (ATCC) CCL-125] were cultured at 27.5°C in Schneider's insect medium (Gibco) supplemented with 10% fetal bovine serum (FBS; Gibco). The *A. albopictus* cell line C6/36 (ATCC CRL-1660) was cultured in RPMI 1640 (Thermo Fisher Scientific) medium containing 10% FBS at 27.5°C. HEK293T and BHK-21 cells were commercially obtained from ATCC and maintained in Dulbecco's modified Eagle's medium (DMEM) (Gibco) supplemented with 10% FBS (Gibco), penicillin (100 U/ml), and streptomycin (100 μg/ml) at 37°C in a humidified atmosphere with 5% CO_2. The 293T-NoDice cell line was provided by B. R. Cullen (Durham, NC, USA).

Primary MLFs were isolated from WT or *Ifnar1*$^{-/-}$ C57/B6 mice as described (*16*). Briefly, lungs were minced and digested in calcium- and magnesium-free Hanks' balanced salt solution (HBSS) buffer (Thermo Fisher Scientific) supplemented with type II collagenase (10 mg/ml; Worthington) and deoxyribonuclease I (20 μg/ml; Sigma-Aldrich) for 3 hours at 37°C with shaking. Cell suspensions were filtered through progressively smaller cell strainers (100 to 40 μm). Filtered cells were plated by using DMEM containing 10% FBS, 2 mM L-glutamine, penicillin (100 U/ml), and streptomycin (100 μg/ml). One hour later, adherent MLFs were rinsed with HBSS and cultured for the subsequent experiments. For knockdown of Dicer, WT or *Ifnar1*$^{-/-}$ MLFs were transfected with siRNAs targeting the ORF of mouse *dicer* gene as previously described (*16*). One day after transfection, MLFs were reseeded and then infected with WT or mutant viruses, respectively.

Plasmids and RNAs

For the reversal-of-silencing assay in *Drosophila* S2 and mosquito Aag2 cells, the EGFP reporter gene, FHV B2 and DENV1-4 viral proteins were constructed into the insect expressing vector pAc5.1/V5-HisB as previously described (*16*). The 400-nt dsRNA for EGFP silencing in S2 or Aag2 cells were generated by in vitro transcription as described (*16*). The 500-nt dsRNAs for knockdown of Dicer-2 and AGO2 of S2 and Aag2 cells were described previously (*16*, *44*). Full-length complementary DNA (cDNA) of FHV RNA1 and RNA1-ΔB2 (T2739C and C2910A) encoded in $CuSO_4$-induced pMT vector were provided by S.-w. Ding (Riverside, CA, USA). Mutations were introduced into the DENV2 NS2A coding region by polymerase chain

reaction (PCR)–mediated mutagenesis with appropriate primers containing the desired nucleotide changes.

For the reversal-of-silencing assay in mammals, the plasmid pEGFP-C1 and the EGFP-specific shRNA were used, as described (*16*). The flaviviral (DENV1-4, JEV, ZIKV, and WNV) NS2A were cloned into mammalian expression vector pRK-Flag/His (provided by H.-B. Shu, Wuhan, China). Plasmids for the purification of MBP fusion protein NS2A and its mutants were constructed by inserting NS2A ORF into a pMAL-c2X vector. The primers used in this study are shown in table S2.

Construction and recovery of mutant viruses

R94A and K135A mutations in DENV2 NS2A were introduced into the infectious DENV2 cDNA clone of strain TSV01 (*45*) (provided by P.-Y. Shi, University of Texas Medical Branch) by PCR-mediated site-directed mutagenesis. R140A mutation in JEV NS2A was introduced into the infectious JEV cDNA clone of SA-E70 (*46*) (a chimeric JEV strain where the prM-E gene of SA14-14-2 is replaced with that of SA14). The positive clones confirmed by sequencing were linearized and then subjected to in vitro transcription by using T7 RNA polymerase (Promega). RNA transcripts were then transfected into C6/36 cells with Lipofectamine 3000, and the rescued viruses were harvested 3 to 4 days after transfection. All the rescued WT and mutant viruses were amplified in C6/36 cells. Viruses were concentrated by Amicon Ultra-15 filters (Millipore), and the titers of viruses were measured by plaque assays.

Plaque assays

Plaque assays were performed on BHK-21 cells in 12-well plates infected with a 10-fold serial dilution of viruses. The plates were incubated at 37°C for 1 hour to allow adsorption. Then, the supernatant was removed, and cells were overlaid with 1% low–melting point agarose (Sigma-Aldrich) in DMEM containing 2% FBS. After further incubation at 37°C for 5 days, the cells were fixed with 4% formaldehyde and stained with 0.2% crystal violet to visualize the plaques.

RNA extraction, Northern blotting, and quantitative reverse transcription PCR

Total RNAs were extracted using TRIzol reagent (Thermo Fisher Scientific) according to the manufacturer's instructions. For the samples required for detection of both viral siRNAs and viral genomic RNAs, small RNA–enriched total RNAs were isolated using the miRNeasy Mini kit (Qiagen) according to the manufacturer's instructions. For Northern blot analysis of high–molecular weight RNA, 5 μg of total RNAs was resolved on denaturing 1.5% agarose gels with 2.2 M formaldehyde, capillary-transferred to a Hybond-A nylon membrane (GE Healthcare). Equal loading was verified before transfer by ethidium bromide staining of total RNA within the RNA gels. For Northern blot analysis of low–molecular weight RNA, 20 μg of total RNAs was resolved on 7 M urea–15% polyacrylamide gel electrophoresis (PAGE), transferred to Hybond-A nylon membrane (GE Healthcare), and chemically cross-linked using 1-ethyl-3-(3-dimethylaminopropyl) carbodiimide. The probe for detection of EGFP mRNA was complementary to the 500 to 720 nt of EGFP ORF. The probe for detection of DENV2 siRNA was complementary to the 150 to 200 nt of antigenomic RNA. For detection of small RNAs, DIG-labeled oligo RNA probes targeting EGFP siRNA, miR-92a, miR-21, and U6 were synthesized by Takara as previously described (*16*). Quantitative reverse transcription PCR (qRT-PCR) was performed with the primers targeting EGFP ORF or DENV2 genome.

Western blotting

Cells were harvested in cell lysis buffer [50 mM tris-HCl (pH 7.4), 150 mM NaCl, 1% NP-40, 0.25% deoxycholate, and a protease inhibitor cocktail (Roche)], and the lysates were then subjected to SDS-PAGE and Western blotting.

Expression and purification of recombinant proteins, gel shift, and in vitro Dicer cleavage assays

For expression and purification of recombinant MBP-fusion proteins, MBP-NS2A and its mutants as well as the negative control protein MBP were expressed in *Escherichia coli* strain TB1 at 27°C in the presence of 0.1 mM isopropyl-β-D-thiogalactopyranoside. Cell pellets were resuspended in binding buffer [20 mM tris-HCl (pH 7.4), 200 mM NaCl, 1 mM EDTA, 10 mM 2-mercaptoethanol) supplemented with 1.5% Triton X-100 and a protease inhibitor cocktail (Roche). Cells were lysed by sonication, and then debris was removed by centrifugation for 10 min at 11,000*g*. The proteins in the supernatant were purified using amylose resin (New England BioLabs) according to the manufacturer's protocol and concentrated using Amicon Ultra-15 filters (Millipore). All proteins were quantified via an ultraviolet-visible spectrophotometer (Shimadzu).

For gel shift assay, MBP-fusion proteins (4 to 16 μM) were incubated with a 0.05 μM DIG-labeled 200-nt dsRNA probe in a binding buffer [50 mM Hepes (pH 8.0), 15 mM NaCl, 0.5 mM $MgCl_2$, 10% glycerol, and 1 U of ribonuclease (RNase) inhibitor (Promega)] at 27°C for 30 min; the total volume was 10 μl. After the binding reaction, the samples were analyzed via 6% native PAGE in 0.5× tris-borate-EDTA (TBE) buffer and transferred to a Hybond-A nylon membrane (GE Healthcare). The membranes were incubated for 30 min with anti-DIG antibody conjugated with alkaline phosphatase (Roche). The RNA probe representing the 1 to 200 nt of EGFP was labeled with DIG–uridine-5′-triphosphate (UTP) (Roche) for in vitro transcription.

For the in vitro Dicer cleavage assay, 0.4 μg of 200-nt dsRNA was incubated with 0.5 U of a recombinant hDicer enzyme (T510002, Genlantis) and MBP-fusion proteins at 37°C for 12 hours. The Dicer-treated RNAs were purified by using TRIzol reagent (Thermo Fisher Scientific) and then separated on 7 M urea–15% PAGE; the RNAs were visualized by staining with ethidium bromide.

CRISPR-Cas9 KO

The IFN-α/βRα CRISPR-Cas9 KO and IFN-α/βRα homology directed repair (HDR) plasmids (sc-401662 and sc-401662-HDR, Santa Cruz Biotechnology) was used to knockout *ifnar1* gene in 293T and 293T-NoDice cells according to the manufacturer's protocol. Briefly, after transfection with the CRISPR-Cas9 KO and HDR plasmids, cells were allowed to be cultured for 3 days, selected by puromycin (1 μg/ml) (Invivogen) and single-cell sorting. The resulting clones were confirmed by DNA sequencing and Western blotting.

RNA-immunoprecipitation

RNA-IP was performed, as previously described with minor modification (*16*). Briefly, cells were lysed in a lysis buffer [20 mM tris-HCl (pH 7.4), 200 mM NaCl, 2.5 mM $MgCl_2$, 1% NP-40, RNase inhibitor (1 U/μl; Promega), and a protease inhibitor cocktail (Roche)]. After centrifugation, the postnuclear lysates were precleared via incubation

with protein-A/G agarose beads (Roche) together with goat anti-mouse immunoglobulin G at 4°C for 4 hours. Then, the precleared lysates were incubated with anti–pan-AGO antibody, together with protein-A/G agarose beads (Roche) at 4°C for 12 hours. The antibody-bound complexes were washed five times with the same lysis buffer except that NaCl concentration was raised to 600 mM. Last, RNAs or proteins were extracted from the complexes and subjected to Northern or Western blotting as described above.

Deep sequencing and data analysis

Libraries of small RNAs from cell culture were constructed using TruSeq Small RNA Library Preparation Kits (Illumina) according to the manufacturer's instructions. The libraries were sequenced by Illumina HiSeq 2000 at RiboBio. The sequencing reads were mapped to the human genome (release hg19) or mosquito genome (AaeGL5.0) by using Bowite 2.2.5, and the cellular miRNA expression level was determined on the basis of the number of reads that was identical to the annotated miRNA sequences in miRBase version 18, only allowing −2 or +2 nt to be templated by the corresponding genomic sequence at the 3′-end. vsRNA reads that cannot be mapped to human genome were then mapped to DENV2 genome with 100% identity. The subsequent analysis of length and location of these vsRNAs were calculated using in-house Perl scripts. Pairs of complementary 22-nt vsRNAs in each library in different distance categories were computed using principles as previously described (*16*, *17*).

Mouse experiments

Groups of 3-week-old *Ifnargr*$^{-/-}$ (AG6) mice or 1-day-old Balb/C mice were inoculated by intracerebral injection with 1×10^4 or 4×10^5 PFU of viruses, respectively. Animals were monitored for 15 days after inoculation. Any mice found in a moribund condition were euthanized and scored as dead. Mouse brains were collected at 3 and 6 dpi, homogenized, and diluted with phosphate-buffered saline to make final 10% (w/v) suspensions. The viral RNAs in brains were measured by qRT-PCR. All animal experiments were performed in strict accordance with the guidelines of the Chinese Regulations of Laboratory Animals (Ministry of Science and Technology of China) and approved by the Institutional Animal Care and Use Committees at Beijing Institute of Microbiology and Epidemiology, Academy of Military Medical Sciences, and Wuhan Institute of Virology, Chinese Academy of Sciences (CAS).

Quantification and statistical analysis

GraphPad Prism was used for all statistical analyses. All experiments were repeated at least three times. Statistical analysis was carried out by unpaired *t* test or two-way analysis of variance (ANOVA) (GraphPad Prism). *P* value <0.05 was considered statistically significant.

Data and software availability

The RNA sequencing data have been deposited to the National Center for Biotechnology Information Gene Expression Omnibus database under the accession number GSE133284.

SUPPLEMENTARY MATERIALS

Supplementary material for this article is available at http://advances.sciencemag.org/cgi/content/full/6/6/eaax7989/DC1

Fig. S1. DENV2 NS2A suppresses RNAi in S2 cells.
Fig. S2. DENV2 NS2A has dsRNA-binding activity that is required to suppress Dicer cleavage in vitro.
Fig. S3. The analyses of DENV2-derived vsiRNAs in 293T-IFNAR1-KO cells.
Fig. S4. VSR deficiency causes replication and infection defects in DENV2-infected mice.
Fig. S5. The knockdown of aaDicer2 and aaAGO2 in Aag2 cells and the conserved active site residues among different AGO proteins.
Fig. S6. NS2As from the four DENV serotypes suppress RNAi in S2 and Aag2 cells.
Fig. S7. Flaviviral NS2As suppress RNAi in 293T cells.
Fig. S8. JEV NS2A inhibits antiviral RNAi in both mosquito and human somatic cells.
Table S1. Profiles of vsRNAs.
Table S2. The primers used in this study.

View/request a protocol for this paper from *Bio-protocol*.

REFERENCES AND NOTES

1. J. S. Mackenzie, D. J. Gubler, L. R. Petersen, Emerging flaviviruses: The spread and resurgence of Japanese encephalitis, West Nile and dengue viruses. *Nat. Med.* **10**, S98–S109 (2004).
2. H. Xia, Y. Wang, E. Atoni, B. Zhang, Z. Yuan, Mosquito-associated viruses in China. *Virol. Sin.* **33**, 5–20 (2018).
3. WHO, Ten threats to global health in 2019 (2019); www.who.int/emergencies/ten-threats-to-global-health-in-2019.
4. D. Baud, D. J. Gubler, B. Schaub, M. C. Lanteri, D. Musso, An update on Zika virus infection. *Lancet* **390**, 2099–2109 (2017).
5. C. A. Daep, J. L. Muñoz-Jordán, E. A. Eugenin, Flaviviruses, an expanding threat in public health: Focus on dengue, West Nile, and Japanese encephalitis virus. *J. Neurovirol.* **20**, 539–560 (2014).
6. X. Pang, R. Zhang, G. Cheng, Progress towards understanding the pathogenesis of dengue hemorrhagic fever. *Virol. Sin.* **32**, 16–22 (2017).
7. S. W. Ding, RNA-based antiviral immunity. *Nat. Rev. Immunol.* **10**, 632–644 (2010).
8. Z. Guo, Y. Li, S. W. Ding, Small RNA-based antimicrobial immunity. *Nat. Rev. Immunol.* **19**, 31–44 (2019).
9. S. W. Ding, Q. Han, J. Wang, W. X. Li, Antiviral RNA interference in mammals. *Curr. Opin. Immunol.* **54**, 109–114 (2018).
10. Q. Wu, X. Wang, S. W. Ding, Viral suppressors of RNA-based viral immunity: Host targets. *Cell Host Microbe* **8**, 12–15 (2010).
11. B. R. Cullen, S. Cherry, B. R. tenOever, Is RNA interference a physiologically relevant innate antiviral immune response in mammals? *Cell Host Microbe* **14**, 374–378 (2013).
12. P. V. Maillard, A. G. van der Veen, E. Z. Poirier, C. Reis E Sousa, Slicing and dicing viruses: Antiviral RNA interference in mammals. *EMBO J.* **38**, e100941 (2019).
13. B. R. Cullen, RNA interference in mammals: The virus strikes back. *Immunity* **46**, 970–972 (2017).
14. P. V. Maillard, C. Ciaudo, A. Marchais, Y. Li, F. Jay, S. W. Ding, O. Voinnet, Antiviral RNA interference in mammalian cells. *Science* **342**, 235–238 (2013).
15. Y. P. Xu, Y. Qiu, B. Zhang, G. Chen, Q. Chen, M. Wang, F. Mo, J. Xu, J. Wu, R. R. Zhang, M. L. Cheng, N. N. Zhang, B. Lyu, W. L. Zhu, M. H. Wu, Q. Ye, D. Zhang, J. H. Man, X. F. Li, J. Cui, Z. Xu, B. Hu, X. Zhou, C. F. Qin, Zika virus infection induces RNAi-mediated antiviral immunity in human neural progenitors and brain organoids. *Cell Res.* **29**, 265–273 (2019).
16. Y. Qiu, Y. Xu, Y. Zhang, H. Zhou, Y. Q. Deng, X. F. Li, M. Miao, Q. Zhang, B. Zhong, Y. Hu, F. C. Zhang, L. Wu, C. F. Qin, X. Zhou, Human virus-derived small RNAs can confer antiviral immunity in mammals. *Immunity* **46**, 992–1004.e5 (2017).
17. Y. Li, M. Basavappa, J. Lu, S. Dong, D. A. Cronkite, J. T. Prior, H. C. Reinecker, P. Hertzog, Y. Han, W. X. Li, S. Cheloufi, F. V. Karginov, S. W. Ding, K. L. Jeffrey, Induction and suppression of antiviral RNA interference by influenza A virus in mammalian cells. *Nat. Microbiol.* **2**, 16250 (2016).
18. Y. Li, J. Lu, Y. Han, X. Fan, S. W. Ding, RNA interference functions as an antiviral immunity mechanism in mammals. *Science* **342**, 231–234 (2013).
19. M. Varjak, C. L. Donald, T. J. Mottram, V. B. Sreenu, A. Merits, K. Maringer, E. Schnettler, A. Kohl, Characterization of the Zika virus induced small RNA response in Aedes aegypti cells. *PLOS Negl. Trop. Dis.* **11**, e0006010 (2017).
20. M. A. Saldaña, K. Etebari, C. E. Hart, S. G. Widen, T. G. Wood, S. Thangamani, S. Asgari, G. L. Hughes, Zika virus alters the microRNA expression profile and elicits an RNAi response in Aedes aegypti mosquitoes. *PLOS Negl. Trop. Dis.* **11**, e0005760 (2017).
21. E. M. Morazzani, M. R. Wiley, M. G. Murreddu, Z. N. Adelman, K. M. Myles, Production of virus-derived ping-pong-dependent piRNA-like small RNAs in the mosquito soma. *PLOS Pathog.* **8**, e1002470 (2012).
22. J. C. Scott, D. E. Brackney, C. L. Campbell, V. Bondu-Hawkins, B. Hjelle, G. D. Ebel, K. E. Olson, C. D. Blair, Comparison of dengue virus type 2-specific small RNAs from RNA interference-competent and -incompetent mosquito cells. *PLOS Negl. Trop. Dis.* **4**, e848 (2010).
23. H. Li, W. X. Li, S. W. Ding, Induction and suppression of RNA silencing by an animal virus. *Science* **296**, 1319–1321 (2002).
24. E. M. Kennedy, A. W. Whisnant, A. V. Kornepati, J. B. Marshall, H. P. Bogerd, B. R. Cullen, Production of functional small interfering RNAs by an amino-terminal deletion mutant of human Dicer. *Proc. Natl. Acad. Sci. U.S.A.* **112**, E6945–E6954 (2015).

25. R. H. Wu, M. H. Tsai, D. Y. Chao, A. Yueh, Scanning mutagenesis studies reveal a potential intramolecular interaction within the C-terminal half of dengue virus NS2A involved in viral RNA replication and virus assembly and secretion. *J. Virol.* **89**, 4281–4295 (2015).
26. H. Xia, H. Luo, C. Shan, A. E. Muruato, B. T. D. Nunes, D. B. A. Medeiros, J. Zou, X. Xie, M. I. Giraldo, P. F. C. Vasconcelos, S. C. Weaver, T. Wang, R. Rajsbaum, P.-Y. Shi, An evolutionary NS1 mutation enhances Zika virus evasion of host interferon induction. *Nat. Commun.* **9**, 414 (2018).
27. Y. C. Tu, C. Y. Yu, J. J. Liang, E. Lin, C. L. Liao, Y. L. Lin, Blocking double-stranded RNA-activated protein kinase PKR by Japanese encephalitis virus nonstructural protein 2A. *J. Virol.* **86**, 10347–10358 (2012).
28. W. J. Liu, X. J. Wang, D. C. Clark, M. Lobigs, R. A. Hall, A. A. Khromykh, A single amino acid substitution in the West Nile virus nonstructural protein NS2A disables its ability to inhibit alpha/beta interferon induction and attenuates virus virulence in mice. *J. Virol.* **80**, 2396–2404 (2006).
29. J. M. Mackenzie, A. A. Khromykh, M. K. Jones, E. G. Westaway, Subcellular localization and some biochemical properties of the flavivirus Kunjin nonstructural proteins NS2A and NS4A. *Virology* **245**, 203–215 (1998).
30. X. Xie, S. Gayen, C. Kang, Z. Yuan, P. Y. Shi, Membrane topology and function of dengue virus NS2A protein. *J. Virol.* **87**, 4609–4622 (2013).
31. X. Zhang, X. Xie, J. Zou, H. Xia, C. Shan, X. Chen, P. Y. Shi, Genetic and biochemical characterizations of Zika virus NS2A protein. *Emerg. Microbes Infect.* **8**, 585–602 (2019).
32. K. J. Yoon, G. Song, X. Qian, J. Pan, D. Xu, H. S. Rho, N. S. Kim, C. Habela, L. Zheng, F. Jacob, F. Zhang, E. M. Lee, W. K. Huang, F. R. Ringeling, C. Vissers, C. Li, L. Yuan, K. Kang, S. Kim, J. Yeo, Y. Cheng, S. Liu, Z. Wen, C. F. Qin, Q. Wu, K. M. Christian, H. Tang, P. Jin, Z. Xu, J. Qian, H. Zhu, H. Song, G. L. Ming, Zika-virus-encoded NS2A disrupts mammalian cortical neurogenesis by degrading adherens junction proteins. *Cell Stem Cell* **21**, 349–358.e6 (2017).
33. R. H. Wu, M. H. Tsai, K. N. Tsai, J. N. Tian, J. S. Wu, S. Y. Wu, J. H. Chern, C. H. Chen, A. Yueh, Mutagenesis of dengue virus protein NS2A revealed a novel domain responsible for virus-induced cytopathic effect and interactions between NS2A and NS2B transmembrane segments. *J. Virol.* **91**, e01836-16 (2017).
34. E. Schnettler, M. G. Sterken, J. Y. Leung, S. W. Metz, C. Geertsema, R. W. Goldbach, J. M. Vlak, A. Kohl, A. A. Khromykh, G. P. Pijlman, Noncoding flavivirus RNA displays RNA interference suppressor activity in insect and mammalian cells. *J. Virol.* **86**, 13486–13500 (2012).
35. P. K. Kakumani, S. S. Ponia, R. K. S, V. Sood, M. Chinnappan, A. C. Banerjea, G. R. Medigeshi, P. Malhotra, S. K. Mukherjee, R. K. Bhatnagar, Role of RNA interference (RNAi) in dengue virus replication and identification of NS4B as an RNAi suppressor. *J. Virol.* **87**, 8870–8883 (2013).
36. G. H. Samuel, M. R. Wiley, A. Badawi, Z. N. Adelman, K. M. Myles, Yellow fever virus capsid protein is a potent suppressor of RNA silencing that binds double-stranded RNA. *Proc. Natl. Acad. Sci. U.S.A.* **113**, 13863–13868 (2016).
37. E. M. Kennedy, A. V. Kornepati, H. P. Bogerd, B. R. Cullen, Partial reconstitution of the RNAi response in human cells using Drosophila gene products. *RNA* **23**, 153–160 (2017).
38. N. K. Sinha, J. Iwasa, P. S. Shen, B. L. Bass, Dicer uses distinct modules for recognizing dsRNA termini. *Science* **359**, 329–334 (2018).
39. P. V. Maillard, A. G. Van der Veen, S. Deddouche-Grass, N. C. Rogers, A. Merits, C. Reis e Sousa, Inactivation of the type I interferon pathway reveals long double-stranded RNA-mediated RNA interference in mammalian cells. *EMBO J.* **35**, 2505–2518 (2016).
40. G. J. Seo, R. P. Kincaid, T. Phanaksri, J. M. Burke, J. M. Pare, J. E. Cox, T. Y. Hsiang, R. M. Krug, C. S. Sullivan, Reciprocal inhibition between intracellular antiviral signaling and the RNAi machinery in mammalian cells. *Cell Host Microbe* **14**, 435–445 (2013).
41. A. G. van der Veen, P. V. Maillard, J. M. Schmidt, S. A. Lee, S. Deddouche-Grass, A. Borg, S. Kjaer, A. P. Snijders, C. Reis e Sousa, The RIG-I-like receptor LGP2 inhibits Dicer-dependent processing of long double-stranded RNA and blocks RNA interference in mammalian cells. *EMBO J.* **37**, e97479 (2018).
42. S. Schuster, L. E. Tholen, G. J. Overheul, F. J. M. van Kuppeveld, R. P. van Rij, Deletion of cytoplasmic double-stranded RNA sensors does not uncover viral small interfering RNA production in human cells. *mSphere* **2**, e00333-17 (2017).
43. X. Xie, P. Y. Shi, Anti-Zika virus RNAi in neural progenitor cells. *Cell Res.* **29**, 261–262 (2019).
44. I. Sanchez-Vargas, J. C. Scott, B. K. Poole-Smith, A. W. Franz, V. Barbosa-Solomieu, J. Wilusz, K. E. Olson, C. D. Blair, Dengue virus type 2 infections of Aedes aegypti are modulated by the mosquito's RNA interference pathway. *PLOS Pathog.* **5**, e1000299 (2009).
45. G. Zou, Y. L. Chen, H. Dong, C. C. Lim, L. J. Yap, Y. H. Yau, S. G. Shochat, J. Lescar, P. Y. Shi, Functional analysis of two cavities in flavivirus NS5 polymerase. *J. Biol. Chem.* **286**, 14362–14372 (2011).
46. S. H. Li, H. Dong, X. F. Li, X. Xie, H. Zhao, Y. Q. Deng, X. Y. Wang, Q. Ye, S. Y. Zhu, H. J. Wang, B. Zhang, Q. B. Leng, R. Zuest, E. D. Qin, C. F. Qin, P. Y. Shi, Rational design of a flavivirus vaccine by abolishing viral RNA 2'-O methylation. *J. Virol.* **87**, 5812–5819 (2013).

Acknowledgments: We thank B. R. Cullen (Durham, NC, USA), H.-B. Shu (Wuhan, China), P.-Y. Shi (Galveston, TX, USA), and S.-w. Ding (Riverside, CA, USA) for reagents. **Funding:** This work was supported by the Strategic Priority Research Program of CAS (XDB29010300 to X.Z.), the National Key Research and Development Project of China (2016YFD0500304 to C.-F.Q.), the National Science and Technology Major Project of China (2018ZX10101004 to X.Z. and 2017ZX10304402 to C.-F.Q.), and the National Natural Science Foundation of China (31761130075 and 31670161 to X.Z., 81661130162 and 81621005 to C.-F.Q., and 81873964 to Y.Q.). X.Z. and C.-F.Q. are supported by the Newton Advanced Fellowship from the Academy of Medical Sciences, UK, and J.C. is supported by funding from the CAS Pioneer Hundred Talents Program. **Author contributions:** Y.Q. and Y.-P.X. performed experiments, with the help of M.M., H.Z., J.X., J.K., D.Z., R.-T.L., R.-R.Z., Y.G., and X.-F.L. Y.Q., M.W., and J.C. analyzed the sequencing data. J.C. helped with experimental design and data interpretation. Y.Q., C.-F.Q., and X.Z. designed the overall study, analyzed the data, and wrote the paper. **Competing interests:** The authors declare that they have no competing interests. **Data and materials availability:** All data needed to evaluate the conclusions in the paper are present in the paper and/or the Supplementary Materials. Additional data related to this paper may be requested from the authors.

Submitted 24 April 2019
Accepted 22 November 2019
Published 5 February 2020
10.1126/sciadv.aax7989

Citation: Y. Qiu, Y.-P. Xu, M. Wang, M. Miao, H. Zhou, J. Xu, J. Kong, D. Zheng, R.-T. Li, R.-R. Zhang, Y. Guo, X.-F. Li, J. Cui, C.-F. Qin, X. Zhou, Flavivirus induces and antagonizes antiviral RNA interference in both mammals and mosquitoes. *Sci. Adv.* **6**, eaax7989 (2020).